

On the study of Galactic potential via action-based mono-abundance stars distribution function

Yuan-Sen Ting,^{1,2*} Hans-Walter Rix,² Jo Bovy,^{3†} Glenn van de Ven,²

¹*Harvard-Smithsonian Center for Astrophysics, 60 Garden Street, Cambridge, Massachusetts 02139, USA*

²*Max Planck Institute for Astronomy, Königstuhl 17, D-69117 Heidelberg, Germany*

³*Institute for Advanced Study, Einstein Drive, Princeton, NJ 08540, USA*

In original form 2012 November 29

ABSTRACT

We present a rigorous and practical way of constraining the Galactic potential based on the phase-space information for many individual stars. Such an approach is needed to dynamically model the data from ongoing spectroscopic surveys of the Galaxy and in the future Gaia. This approach describes the orbit distribution of stars by a family of parametrized distribution function (DF) proposed by McMillan & Binney, which are based on actions. We find that these parametrized DFs are flexible enough to capture well the observed phase-space distributions of individual abundance-selected Galactic sub-populations of stars (‘mono-abundance populations’) for a disc-like gravitational potential, which enables independent dynamical constraints from each of the Galactic mono-abundance populations.

We lay out a statistically rigorous way to constrain the Galactic potential parameters by constructing the joint likelihood of potential and DF parameters, and subsequently marginalizing over the DF parameters. This approach explicitly incorporates the spatial selection function inherent to all Galactic surveys, and can account for the uncertainties of the individual position-velocity observations.

On that basis, we study the precision of the parameters of the Galactic potential with that can be reached with various sample sizes and realistic spatial selection functions. By creating mock samples from the DF, we show that, even under a restrictive and realistic spatial selection function, one can recover the true potential parameters to a few per cent with sample sizes of a few thousands. The assumptions of axisymmetry, DFs that are smooth in the actions and no time-variation remain important limitations in the approach.

Key words: Galaxy: disc — Galaxy: fundamental parameters — Galaxy: halo — Galaxy: kinematics and dynamics — Galaxy: structure

1 INTRODUCTION

Constraining the Galactic potential optimally has been a very difficult yet important aspect of studies of the Milky Way and the Local Group. Understanding the various components of the Galactic potential, for instance separating the potential contributions from the baryonic disc and that from the dark matter halo is fundamental to understanding the history and formation of our own Galaxy. Furthermore, understanding the dark halo potential near the Sun is a crucial step to pin down the density and thus the scattering cross-section of the dark matter, which in turn is crucial in-

put for interpreting any dark-matter annihilation signal at the centre of Milky Way (e.g. Su & Finkbeiner 2012).

In the past few decades, constraining the Galactic potential has mostly relied on the Jeans equation (for a summary, see Binney & Tremaine 2008) despite the known problems of this approach. For instance, one only keeps the velocity dispersion moments up to second order in the Jeans equation. This predicts a Gaussian ellipsoid velocity distributions that does not capture the observed and expected asymmetries in the angular velocity v_ϕ (e.g. Fuchs et al. 2009).

One of the ways to alleviate these problems is through explicitly modelling the stellar population distribution function (DF), either via integrals of motions or actions instead of just taking position-velocity moments, as is the case of the Jeans equation (Dehnen 1999; Binney 2010; Binney & McMillan 2011; McMillan & Binney 2012;

* E-mail: yuan-sen.ting@cfa.harvard.edu

† Hubble fellow

Solway et al. 2012). For such modelling, it is crucial that relatively simple analytic distribution functions, e.g. based on the actions, are reasonably good approximations to the actual orbit distributions for at least sub-populations of stars in the Galactic disc. How well such DF approximations work in practice is not yet clear. To explore this question, we consider in particular stellar sub-populations of a particular age or abundance pattern (Freeman & Bland-Hawthorn 2002; Ting et al. 2012).

Recently Bovy et al. (2012a,b,c) (hereafter, BO12) showed, using G-dwarfs from the *SEGUE* survey (Sloan Extension for Galactic Understanding and Exploration; Yanny et al. 2009), that mono-abundance, stars that have nearly the same [Fe/H] and [α /Fe], populations have very simple (\vec{x}, \vec{v}) phase-space distribution properties: spatial density distributions that vary exponentially, both in the radial and vertical direction; and furthermore, each mono-abundance population shows isothermal velocity dispersion in the vertical direction and exponentially in the radial direction (Bovy et al. 2012c). This simplicity in (\vec{x}, \vec{v}) -space gives hope that one could describe mono-abundance populations with simple action-based DFs which is one of the purposes of this study.

Since stars are the most abundant tracers of the Galactic potential, simple action-based DFs will naturally provide a statistical and rigorous method to constrain the Galactic potential because the conversion of position-velocity variable (configuration space) to the actions-angles variable depends on parameters of the potential (see Binney 2010, 2011; Binney & McMillan 2011; McMillan 2011; Binney 2012; McMillan & Binney 2012, for generic ground-work on the topic). The main idea is to determine the likelihood of the observational data, given a joint set of parameters for both the DF and the gravitational potential; subsequent marginalization over the DF parameters provides then a rigorously derived constraint on the potential. Such an approach appears to be a precondition to fully exploit the dynamical information content of large Galactic surveys that will provide us spatial and velocity distribution, along with elemental abundances, including APOGEE (The Apache Point Observatory Galactic Evolution Experiment; Eisenstein et al 2011), GALAH (Galactic Archaeology survey with HERMES; Freeman 2010, 2012) and ESO-Gaia (Gilmore et al. 2012).

In the context of dynamical modelling the Galactic disc with action-based DFs, the goals of the paper are three-fold: explore how well ‘mono-abundance populations’ can be approximated by simple action-based analytic DFs; lay out a formalism that provides constraints from a set of discrete stellar positions and velocities on the gravitational potential, after marginalizing over the DF; forecast what constraints on the *shape* of the potential we can expect given existing sample sizes.

This paper is organized as follow: in Section 2, we discuss the choice of parametrization of the DF and summarize the adiabatic approximation that we assume to calculate the actions variable efficiently. In Section 3, we will show that our choice of DF exhibits all the basic phase-space distribution properties of mono-abundance stars, with the only caveat that disc potential has to be included in order for the vertical spatial profile to fit. In Section 4, we show that by studying the likelihood of the DF-potential parameters, one

can recover the potential parameters, even under a restrictive and realistic spatial selection function.

Throughout this study, we denote cylindrical coordinate to be $\vec{x} \equiv (R, \phi, z)$. We assume velocities are measured in the inertial Galactocentric frame with axisymmetric potential, $\Phi = \Phi(R, z)$.

2 CHOICE OF DISTRIBUTION FUNCTION

We follow the DF advocated by Binney (2010) and McMillan & Binney (2012) closely, but note that we rearrange some of the terms in the DF to facilitate physical interpretation of the DF. For circular orbits in the equatorial Galactic plane, the DF has to be of the form:

$$f(J_R, L_z, J_z) = \tilde{f}(L_z)\delta(J_R - 0)\delta(J_z - 0) \quad (1)$$

where $\tilde{f}(L_z)$ determines the angular momentum distribution for a infinitely cold planar disc, J_R and J_z are the radial and vertical action, respectively.

In the cold disc limit, the circular radius R_c coincides with the observed radius, where

$$L_z = R_c \cdot V_c(R_c) \quad (2)$$

and V_c is the circular velocity,

$$V_c = \sqrt{R \cdot \frac{\partial \Phi}{\partial R}} \quad (3)$$

Thus we have for an exponential disc, up to a multiplicative normalization constant,

$$\tilde{f}(L_z)dL_z = \exp\left(-\frac{R_c}{h_R}\right)R_c dR_c \quad (4)$$

The DF parameter h_R determines the radial spatial distribution. In a more general setting, we relax the $J_R = J_z = 0$ constraint and propose the DF to be:

$$f(J_R, L_z, J_z) = \tilde{f}(L_z) \left[\frac{\kappa(L_z)}{C_R(L_z)} \exp\left(-\frac{\kappa(L_z)J_R}{C_R(L_z)}\right) \right] \left[\frac{\nu(L_z)}{D_R(L_z)} \exp\left(-\frac{\nu(L_z)J_z}{D_R(L_z)}\right) \right] \quad (5)$$

where

$$C_R(L_z) = \sigma_R \exp\left(-\frac{R_c(L_z)}{h_\sigma}\right) \quad (6)$$

$$D_R(L_z) = \sigma_z \exp\left(-\frac{R_c(L_z)}{h_\sigma}\right) \quad (7)$$

where R_c is the circular radius given angular momentum L_z , assuming equatorial in-plane movement, $\kappa(L_z)$ and $\nu(L_z)$ are the radial and vertical frequency, respectively, under epicycle approximation. The DF parameter h_σ determines the radial exponential decay of the velocity dispersion, whereas σ_R and σ_z control the total radial and vertical dispersion, respectively.

The κ and ν terms are necessary (e.g. Binney 2010) for two reasons:

(i) A finite increment in energy E can lead to an infinite increment of actions in the unbound case. One would love to have a term that will tend to zero at large L_z and couple this term with J_R . One of the possible choices is the radial

frequency $\kappa(R_c(L_z))$. At large R_c , the effective potential is less concave at the minimum point and therefore $\kappa(R_c(L_z))$ tends to zero. Similarly for the vertical frequency.

(ii) Qualitatively, in R_c region where κ changes more drastically, the increment of J_R is also more drastic, and therefore the scale length of J_R has to decrease in proportion to compensate this effect. Similarly for the vertical oscillation.

2.1 Adiabatic approximation

Importantly, we only measure (R, z, v_R, v_ϕ, v_z) but not the actions. In order to study actions-based DF, we employ the adiabatic approximation in order to calculate the radial and vertical actions efficiently.

Binney & McMillan (2011) and Solway et al. (2012) showed that the vertical action J_z calculated in a fixed radius R approximation is almost conserved, even with radial migration, and interferences of spiral(s) or bar. More precisely,

$$J_z \simeq \oint dz \dot{z}(z|R) \quad (8)$$

This reduces the calculation to one-dimensional integration that can be numerically calculated easily. Furthermore, since $\Phi(z|R) = \Phi(-z|R)$, to calculate the approximated vertical action, we have:

$$J_z = \frac{2}{\pi} \int_0^{z_{\max}} dz \sqrt{\dot{z}_{\text{init.}}^2 + 2(\Phi(z_{\text{init.}}|R_{\text{init.}}) - \Phi(z|R_{\text{init.}}))} \quad (9)$$

where the subscript ‘init.’ stands for the observed value in practice.

Similarly, for the radial action, we can consider the radial component at the equatorial plane, ignoring the vertical motion. Under this assumption,

$$J_R = \oint dR \dot{R}(R|z=0) \quad (10)$$

We deduce

$$J_R = \frac{1}{\pi} \int_{R_{\text{peri.}}}^{R_{\text{apo.}}} dR \sqrt{\dot{R}_{\text{init.}}^2 + \frac{L_z^2}{R_{\text{init.}}^2} - \frac{L_z^2}{R^2} + 2(\Phi(R_{\text{init.}}, 0) - \Phi(R, 0))} \quad (11)$$

where $R_{\text{apo.}}$ and $R_{\text{peri.}}$ are the apo- and peri-centric radius, respectively.

2.2 Variation of actions under adiabatic approximation

Fig 1 and Table 1 illustrate the variation of the approximated actions in the course of a trajectory. We assume a Miyamoto-Nagai potential,

$$\Phi(R, z) = -\frac{GM}{\sqrt{R^2 + (a + \sqrt{z^2 + b^2})^2}} \quad (12)$$

with parameter $GM = 7.5 \times 10^5 \text{ km}^2/\text{s}^2 \text{ kpc}$, $a = 5 \text{ kpc}$, $b = 1 \text{ kpc}$. We choose these parameters because we have almost a flat rotation curve at Galactocentric radius 5 kpc < $R < 12 \text{ kpc}$ and circular velocity $V_c(R_\odot) \simeq 220 \text{ km/s}$ at the

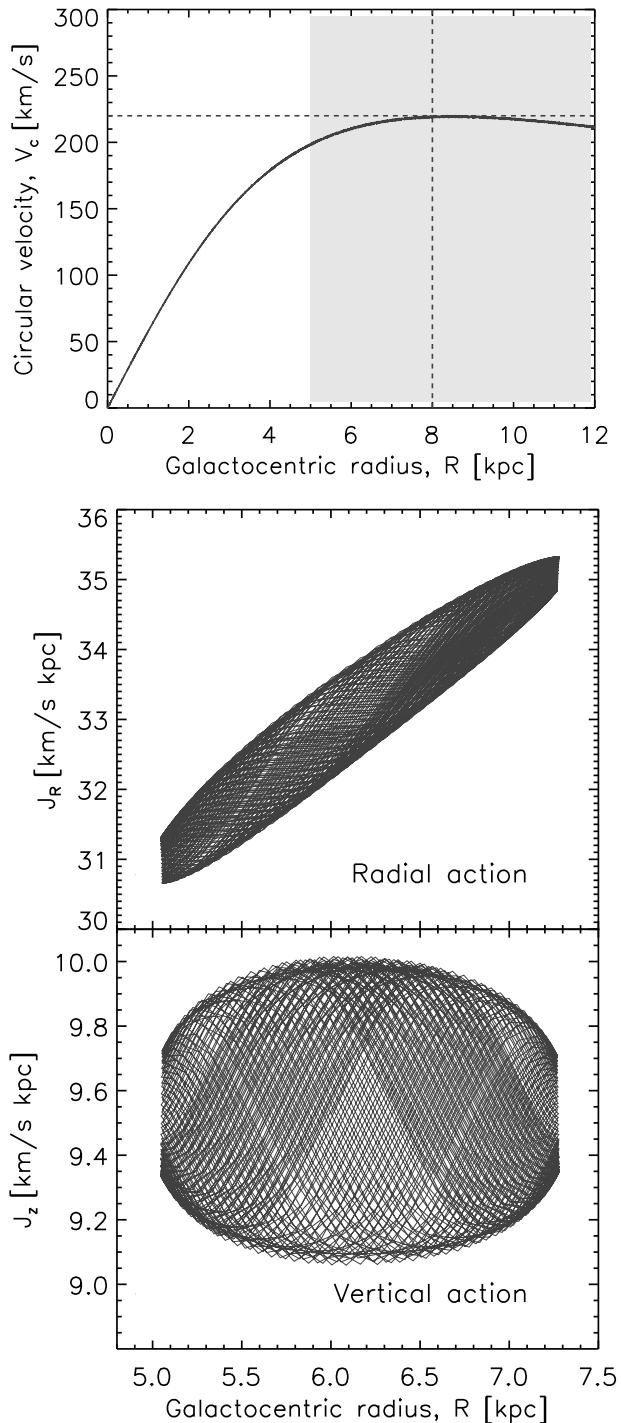


Figure 1. Approximate action calculation in a Miyamoto-Nagai potential: the top panel shows the circular velocity of a Miyamoto-Nagai potential with $GM = 7.5 \times 10^5 \text{ km}^2/\text{s}^2 \text{ kpc}$, $a = 5 \text{ kpc}$, $b = 1 \text{ kpc}$, the vertical dashed line marks approximately the solar Galactocentric radius, the horizontal dashed line indicates the common accepted circular velocity $V_c = 220 \text{ km/s}$ at solar radius and the shaded region shows the region where the circular velocity is approximately constant in this choice of potential; the middle and bottom panel show the variation of actions calculated using adiabatic approximation in the course of trajectory. We plot the case of $R_{\text{init.}} = 6$ in Table 1. The results show that actions calculated with adiabatic approximation are almost conserved along the orbit with less than 5 per cent variation.

Table 1. Variation of actions variable under adiabatic approximation with slight perturbation to the circular orbit under Miyamoto-Nagai potential that gives a flat rotation curve.

$R_{\text{init.}}$ kpc	L_z km/s kpc	$\dot{R}_{\text{init.}}$ km/s	$\dot{z}_{\text{init.}}$ km/s	Δ_{J_R} per cent	Δ_{J_z} per cent
3.	450.	90.	60.	4	3
6.	1250.	60.	40.	5	3
9.	1970.	30.	20.	4	2

solar radius $R_\odot = 8$ kpc as shown in the top panel of Fig 1.

We apply slight perturbation on circular orbits that mimic the radial velocity dispersion of 40 km/s at solar Galactocentric radius, radial to vertical velocity dispersion ratio of $\sqrt{2}$ (Fuchs et al. 2009) and velocity scale length of 3.5 kpc (BO12). We define the variation of action Δ_J to be the one-sigma over the mean value of the action for each time-step. The results of Δ_J are listed in Table 1. The results show that the approximated actions are almost conserved in all cases.

We also examine potential due to double exponential disc (i.e. with density decaying both radially and vertically), and also flattened isothermal potential:

$$\Phi = V_c^2(R_\odot) \ln \sqrt{R^2 + \frac{z^2}{q^2}} \quad (13)$$

The results are qualitatively similar, with the variation of actions less than 5 per cent in all cases. Binney (2012) studies a more precise method of calculating the actions, but as we will show in the results below, it is not necessary for our study purpose.

3 MATCHING THE PHASE-SPACE DISTRIBUTION OF MONO-ABUNDANCES POPULATIONS

In this section, we will show that the DF in equation (5) is a good representation of the observed position-velocity distribution of mono-abundance sub-components of the Milky Way disc, namely that they exhibits an exponential spatial density, both radially and vertically, and an isothermal velocity dispersion in the vertical direction and exponentially decaying in the radial direction.

3.1 Dealing with Jacobian change of measure

In order to have the conversion of DF between canonical position-velocity variable and the actions variable, one has to take care of the Jacobian term carefully. Note that

$$\int d^3\vec{x} d^3\vec{p} \tilde{f}(\vec{x}, \vec{p}) = \int d^3\vec{J} d^3\vec{\theta} f(\vec{J}) \quad (14)$$

where \vec{p} is the canonical momentum associated to \vec{x} . Since (\vec{x}, \vec{p}) , $(\vec{J}, \vec{\theta})$ are canonical variables and measure is invariance under canonical transformation, we have

$$\tilde{f}(\vec{x}, \vec{p}) = f(\vec{J}(\vec{x}, \vec{p})) \quad (15)$$

Furthermore, in cylindrical coordinate, $(p_R, p_\phi, p_z) = (v_R, Rv_\phi, v_z)$, we deduce

$$f(\vec{x}, \vec{v}) = Rf(\vec{J}(\vec{x}, \vec{p}(\vec{x}, \vec{v}))) \quad (16)$$

In summary, for an axisymmetric potential, in order to convert actions-based DF to (\vec{x}, \vec{v}) -space distribution, it suffices to multiply the Jacobian ($= R$) term.

3.2 Fitting the phase-space distribution via maximum-likelihood

We create mock data stellar tracers with (R, z, v_R, v_ϕ, v_z) attributes, such that it has density scale length about 2.5 kpc, dispersion scale length about 3.5 kpc with *Gaussian* velocity dispersion of $\sigma_R = 40$ km/s at solar Galactocentric radius, $\sigma_R/\sigma_z = \sqrt{2}$, $\sigma_R/\sigma_\phi = 1.5$ (Fuchs et al. 2009, BO12). We assume that the mean velocity of the Gaussian for each spatial point

$$\overline{v_R}(R, z) = \overline{v_z}(R, z) = 0 \quad (17)$$

$$\overline{v_\phi}(R, z) = \overline{v_\phi}(R) = V_c(R) - A \frac{\sigma_R^2(R)}{2V_c(R)} \quad (18)$$

where (see Bovy & Tremaine 2012, for details),

$$A = \left(\frac{1}{h_R} + \frac{1}{h_\sigma} \right) \times R - 0.5 \quad (19)$$

We assume that all of the mixed moments ($\sigma_{R\phi}^2$, σ_{Rz}^2 and $\sigma_{\phi z}^2$) vanish. Thus, we assume that both the vertex deviation and the tilt of the velocity ellipsoid are zero, even though these were not measured by BO12. The tilt of the velocity ellipsoid in particular is not expected to be zero at heights $\gtrsim 1$ kpc above the plane (e.g. Siebert et al. 2008). However, as discussed by Binney & McMillan (2011), the adiabatic approximation is unable to capture a non-zero tilt as it assumes that the radial and vertical motions are independent. Thus, even though the quasi-isothermal DF of equation (5) has a non-zero tilt when used with correctly calculated actions (for example, using the torus machinery; Binney & McMillan 2011), it does not when using the adiabatic approximation. For this reason, we assume that the tilt of the velocity ellipsoid is zero in what follows.

We search for the best-fitting DF parameters by maximum likelihood. For this section, we fix a particular choice of Miyamoto-Nagai potential parameters: $GM = 7.5 \times 10^5$ km²/s² kpc, $a = 5$ kpc, $b = 1$ kpc. We examine various choice of the potential parameters. It does not change the results qualitatively. We emphasize that the mock tracers population mimics a mono-abundance population. Note that, the probability that we observe $(\vec{x}_\alpha, \vec{v}_\alpha)$, according to our DF model with DF-parameters $\vec{\lambda}_{\text{DF}}$ is

$$\text{Pr}(\vec{x}_\alpha, \vec{v}_\alpha | \Phi, \vec{\lambda}_{\text{DF}}) = f(\vec{x}_\alpha, \vec{v}_\alpha | \Phi, \vec{\lambda}_{\text{DF}}) \quad (20)$$

Given this probability, we can define the log-likelihood to be the sum over N_α mock data, and search for the best DF-parameters by maximizing the log-likelihood.

$$\ln \mathcal{L}_{\text{DF}}(\vec{\lambda}_{\text{DF}}) \equiv \sum_\alpha \ln[\text{Pr}(\vec{x}_\alpha, \vec{v}_\alpha | \Phi, \vec{\lambda}_{\text{DF}})] \quad (21)$$

We obtain the best-fitting parameters by performing a nested-grid search on the multi-dimensional $\vec{\lambda}_{\text{DF}}$ space

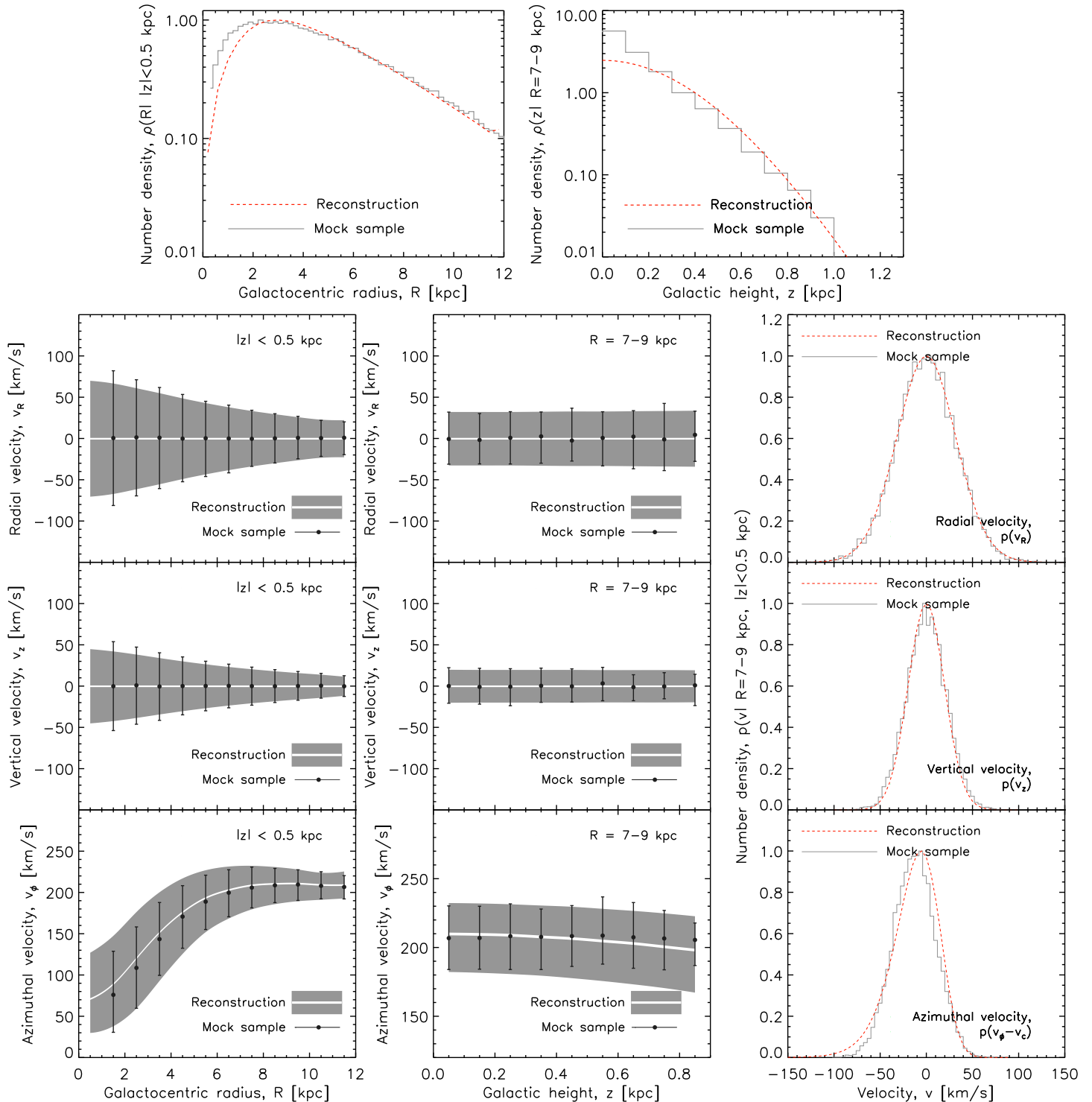


Figure 2. How well can the DF family from equation (5) approximate the observed properties of Galactic mono-abundance stellar sub-populations (BO12) in a Miyamoto-Nagai potential? Those mono-abundance populations have an exponential spatial density, both radially and vertically, and an isothermal velocity dispersion in the vertical direction and exponentially decaying in the radial direction. To create mock data, we assume a radial velocity dispersion about 40 km/s at solar Galactocentric radius and scale height $h_z = 0.18$ kpc for the mock data. The top row shows the radial (left) and vertical (right) density distributions in $(R, z) \in [0, 12] \times [-0.5, 0.5]$ kpc 2 and $(R, z) \in [7, 9] \times [0, 1.3]$ kpc 2 , respectively. The dashed red line shows the reconstructed profile from the best-fitting DF and the grey solid histogram shows the mock data. The second row shows the distribution of v_R as a function of R with $z \in [-0.5, 0.5]$ kpc (left panel) and as a function of z with $R \in [7, 9]$ kpc (middle panel), and also the histogram in $(R, z) \in [7, 9] \times [-0.5, 0.5]$ kpc 2 . The grey shaded region shows the reconstructed profile from the best-fitting DF with the white solid line to be median value, whereas the black solid filled circle and their vertical error bars show the results of the mock data. The third and fourth row show the distribution of v_z and v_ϕ , respectively. The DF family fits the tracer population very well for a disc potential.

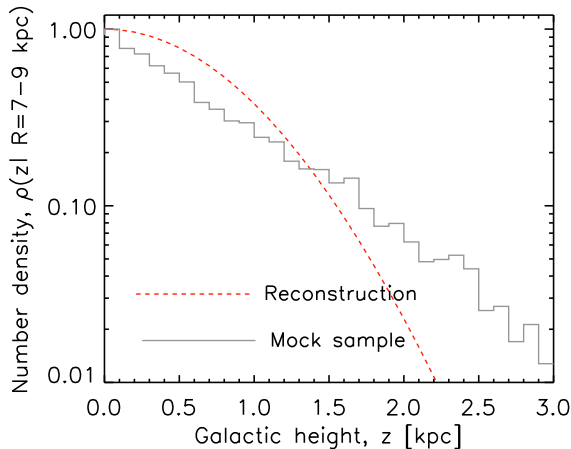


Figure 3. Similar to the top right panel of Fig. 2, but for isothermal potential with the axis ratio $q = 1$ and circular velocity $V_c = 220$ km/s. We also tried various choices of q , but the fits are equally unsatisfactory: the DF family in equation (5) cannot produce a vertically exponential tracer density profile, if stars orbit in a flattened isothermal sphere.

and finding the set of parameters that maximizes the likelihood. After obtaining the best-fitting parameters, we calculate from $f(\vec{J}(\vec{x}, \vec{v}))$ the stellar profile in configuration space (\vec{x}, \vec{v}) and compare it to the one of the mock data to check whether our assumption on the functional form of the DF represents well the mock data. We consider a grid of position-velocity configuration space (R, z, v_R, v_ϕ, v_z) and calculate the DF in configuration space using equation (16). We then calculate the stellar profile of each position-velocity component by marginalizing over the other spatial-velocity components.

Note that, given the functional form of the DF in equation (5), *the predicted vertical profile is fixed by the vertical velocity dispersion and the potential, but independent of the scale height of the mock data.* We find that the vertical profile is predicted satisfactorily with the Miyamoto-Nagai potential (as shown in Fig. 2) but not with the isothermal potential (as shown in Fig. 3).

This can be explained by the following. In the case that $R \gg z$, the vertical restoring force of the Miyamoto-Nagai potential and thus \dot{z} is about constant. This implies that the vertical action is proportional to z , and the vertical profile in ansatz equation (5) goes down exponentially. On the other hand, the vertical restoring force of the isothermal potential and thus \dot{z} is proportional to z . This implies that the vertical action are proportional to z^2 , and the vertical profile will go down too drastically [proportional to $\exp(-z^2)$].

We conclude that the quasi-isothermal DF of equation (5) provides a good representation of the DF of mono-abundance sub-populations of the Milky Way disc. More importantly, the action-based DFs predict a low- v_ϕ tail. As discussed in Section 1, this coincides better with the observation (e.g. Fuchs et al. 2009). In the following section, we will generate mock samples by rejection sampling *directly from the DF*.

4 CONSTRAINING THE GALACTIC POTENTIAL

In this section, we will show that, given a functional form of the potential and the DF, we can recover the optimal potential parameters by marginalizing over the DF parameters. Note that in practice, we only observe a very small part of the Galaxy. For simplicity, we assume that the observed volume is a cylinder around the Galactic center with a finite width and height. Mathematically, we have to include the selection function

$$P_{\text{select}} = \begin{cases} 1, & \text{if } |R - 8| < 1 \text{ kpc and } |z| < 2.5 \text{ kpc} \\ 0, & \text{otherwise} \end{cases} \quad (22)$$

With this selection function in place, given any parameters of the DF and the potential, $\vec{\lambda} \equiv (\vec{\lambda}_{\text{DF}}, \vec{\lambda}_{\text{potential}})$, we carefully normalize the DF through Monte-Carlo integration, more precisely

$$f(\vec{J}|\vec{\lambda}) \longrightarrow \frac{f(\vec{J}|\vec{\lambda})}{\mathcal{N}(\vec{\lambda})} \quad (23)$$

where

$$\mathcal{N}(\vec{\lambda}) = \frac{1}{2\pi} \int d^3\vec{x} d^3\vec{v} R \cdot P_{\text{select}}(R, z) f(\vec{J}(\vec{x}, \vec{v})|\vec{\lambda}) \quad (24)$$

To our best knowledge, this is the first attempt that has never before been implemented to study the joint distribution of DF and potential parameters in the context of constraining the Galactic potential.

First, we consider the two-dimensional in-plane Miyamoto-Nagai potential which contains two potential parameters: GM and a . We consider the case where $h_R = 2.5$ kpc, $h_\sigma = 4$ kpc and $\sigma_R = 12000$ (km/s)³ in equation (5), which roughly mimics the observed velocity distributions from our calculation in Section 3.

We define the likelihood of the potential parameters, $\mathcal{L} = \mathcal{L}(\vec{\lambda}_{\text{potential}})$ by marginalizing over $\vec{\lambda}_{\text{DF}}$. We estimate the one-sigma significance of the best-fitting potential parameter by finding the demarcation line at $2 \ln(\mathcal{L}/\mathcal{L}_{\text{max}}) = 2.7$ and two-sigma significance at $2 \ln(\mathcal{L}/\mathcal{L}_{\text{max}}) = 4.6$. We create data with $GM = 7.5 \times 10^5$ km²/s² kpc, $a = 5$ kpc, $b = 1$ kpc in the observed volume $R = 7 - 9$ kpc and $|z| < 2.5$ kpc.

We reiterate the process for various sample sizes for the mock data, N_{tracers} for the same observed volume. As shown in Fig 4, the one-sigma uncertainty goes down as $1/\sqrt{N_{\text{tracers}}}$. We use the results with the sample size $N_{\text{tracers}} = 30000$ to be our reference, because the uncertainty of the potential parameters is ≤ 0.1 per cent in this case. We show that this reference value coincides with the true value, indicating that, assuming a potential model, we can recover the true potential parameter with observation restricted to a small volume. We show that we can find the best-fitting potential parameters within one- to two-sigma significance from the true value regardless of the sample size.

We extend this results to the three-dimensional case by considering the flattened isothermal potential with two parameters [equation (13)]: V_c and q . We consider the warm-disc case where $h_R = 2.5$ kpc, $h_\sigma = 3.5$ kpc, $\sigma_R = 12000$ (km/s)³, $\sigma_z = 8000$ (km/s)³ for DF in equation (5). We create the mock data from the potential with $V_c = 220$ km/s and $q = 0.8$. As shown in Fig 5, one can recover

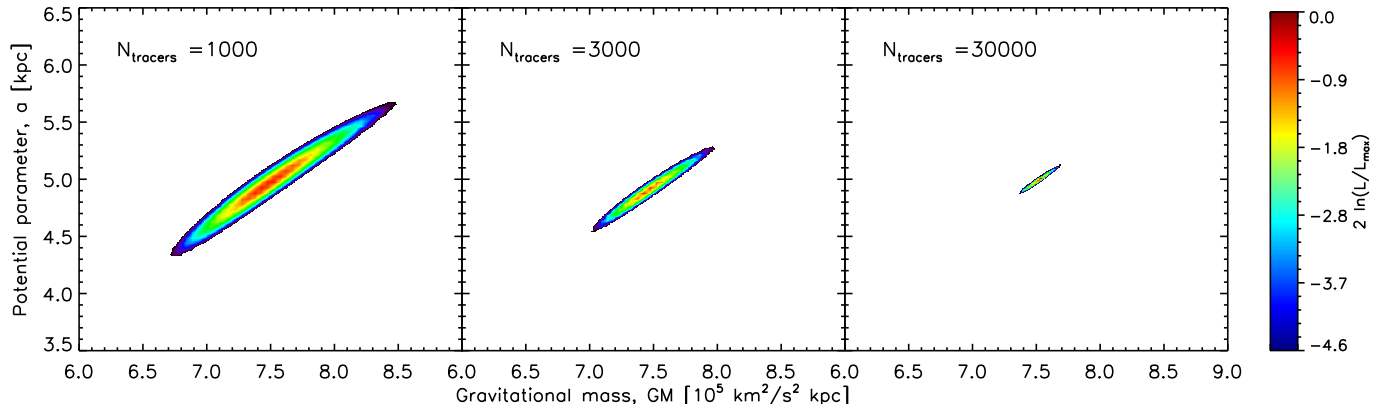


Figure 4. Likelihoods of the data given the parameters of a Miyamoto-Nagai potential, assuming that the N_{tracers} observational constraints are available within $R = 7 - 9$ kpc and $|z| < 2.5$ kpc. We only plot the likelihood region that encloses 95 per cent of the total probability. The left panel shows the results of mock data points $N_{\text{tracers}} = 1000$, the middle panel $N_{\text{tracers}} = 3000$ and the right panel $N_{\text{tracers}} = 30000$: the likelihood contours tighten as $1/\sqrt{N_{\text{tracers}}}$ around the correct input parameters for the mock data. The data constrain a highly degenerate combination of GM and a .

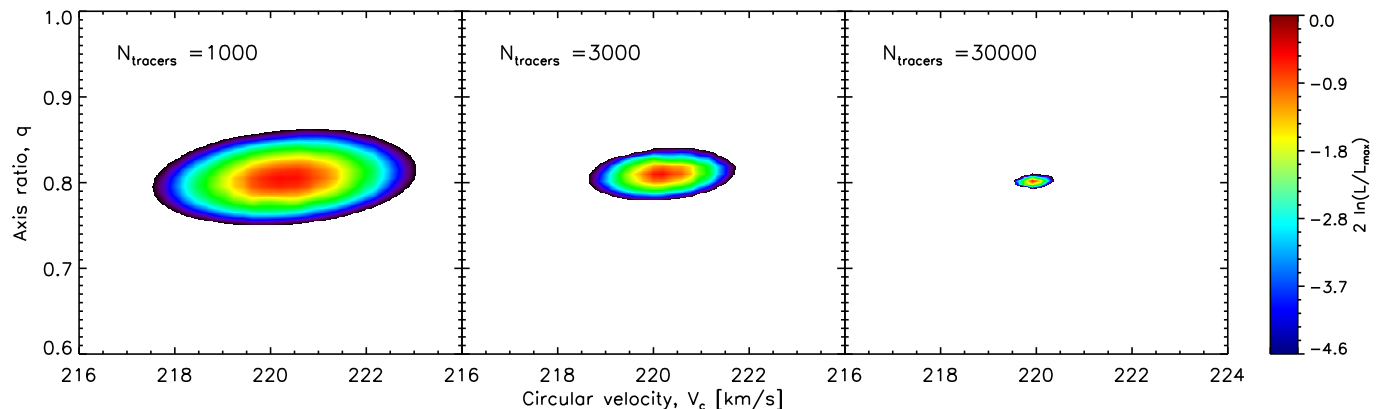


Figure 5. Similar to Fig 4 but for a flattened isothermal potential. Here the estimates for the potential flattening and the circular velocity are hardly correlated.

both the circular velocity V_c and the axis ratio q successfully with our proposed method.

Note that, in most cases, without a Galactic dust-map, observations in the equatorial Galactic disc are less reliable. Therefore, we also tested the more realistic scenario, where the observed volume is restricted to the annulus height of $1 < z < 2.5$ kpc without the mid-plane. The results show that we can about equally well constrain the axis ratio q , given the same sample size. This could be probably due to the fact that our three-dimensional isothermal potential is too restrictive, therefore the axis ratio is not too sensitive to the vertical observed volume restriction. However, the V_c uncertainty is larger, indicating the adiabatic approximation is not as good away from the Galactic plane.

5 CONCLUSIONS

We demonstrate a way to constrain the Galactic potential from mono-abundance stellar populations. We show that the phase-space distribution properties of mono-abundance stars can be fitted very well with simple action-based distri-

bution function. Assuming that the vertical and radial velocity dispersion scale lengths are the same, these properties are fully-determined by only four DF parameters.

We further show that, assuming that the proposed DF is the true representation of the mono-abundance populations and certain parametrization of the Galactic potential, we devise a statistical and rigorous method to measure the Galactic potential parameters. This is achieved by calculating the likelihood of observational data, given a joint set of parameters for both the DF and the gravitational potential and subsequently marginalizing over the DF parameters.

We create mock data sample from the distribution function with various potentials, including the Miyamoto-Nagai in-plane potential and a flattened isothermal potential. We show that even with a mono-abundance sample of the size of a few thousands, we can pin down the potential parameters to a few per cent.

In this study, we assume that the measurement is perfect without uncertainty in the position and velocity measurements. The inclusion of measurement uncertainty should be conceptually straightforward. We will explore this aspect in a future paper.

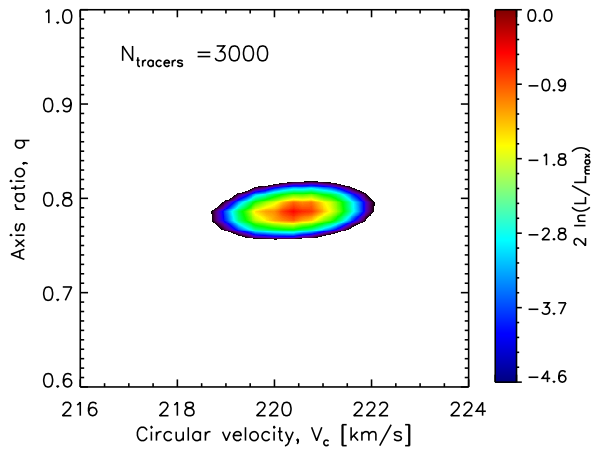


Figure 6. Similar to the middle panel of Fig. 5, but with the vertical range of available tracer constraints restricted to $1 < z < 2.5$ kpc- the mid-plane cut out: this is a more realistic selection function since in most cases, without a Galactic dust-map, observations in the equatorial Galactic disc are less reliable.

Although a more realistic potential, for instance a combination of halo, bulge and disc potential will contain more than two parameters and hence pose a challenge to the estimation, different mono-abundance stars are tracing the same Galactic potential and therefore their joint constraints with the method we propose is still very promising.

ACKNOWLEDGEMENTS

YST and JB are grateful to the Max-Planck Institut für Astronomie for its hospitality and financial support during part of the period during which this research was performed. JB was supported by NASA through Hubble Fellowship grant HST-HF-51285.01 from the Space Telescope Science Institute, which is operated by the Association of Universities for Research in Astronomy, Incorporated, under NASA contract NAS5-26555. JB was partially supported by SFB 881 funded by the German Research Foundation DFG.

REFERENCES

- Binney J., 2010, MNRAS, 401, 2318
 Binney J., 2011, Pramana, 77, 39
 Binney J., 2012, MNRAS, 426, 1324
 Binney J., McMillan P., 2011, MNRAS, 413, 1889
 Binney J., Tremaine S., 2008, Galactic Dynamics. Princeton Univ. Press, New Jersey
 Bovy J., Tremaine S., 2012, ApJ, 756, 89
 Bovy J., Rix H. W., Hogg D. W., 2012a, ApJ, 751, 131
 Bovy J., Rix H. W., Hogg D. W., Beers T. C., Lee Y. S., Zhang L., 2012b, ApJ, 755, 115
 Bovy J., Rix H. W., Liu C., Hogg D. W., Beers T. C., Lee Y. S., 2012c, ApJ, 753, 148
 Dehnen W., 1999, AJ, 118, 1201
 Eisenstein D. et al., 2011, AJ, 142, 72
 Freeman K. C., Bland-Hawthorn J., 2002, ARA&A, 40, 487

- Freeman K. C., 2010, in Block D. L., Freeman K. C., Puerari I., eds, Galaxies and their Masks. Springer-Verlag, Berlin, p. 319
 Freeman K. C., 2012, in Aoki W., Ishigaki M., Suda T., Tsujimoto T., Arimoto N., eds, ASP Conf. Ser. Vol. 458. Astron. Soc. Pac., San Francisco, p. 393
 Fuchs B. et al., 2009, AJ, 137, 4149
 Gilmore G. et al., 2012, The Messenger, 147, 25
 McMillan P. J., 2011, MNRAS, 414, 2446
 McMillan P. J., Binney J., 2012, MNRAS, 419, 2251
 Miyamoto M., Nagai R., 1975, PASJ, 27, 533
 Siebert A. et al., 2008, MNRAS, 391, 793
 Solway M., Sellwood J. A., Schönrich R., 2012, MNRAS, 422, 1363
 Su M., Finkbeiner D. P., 2012, arXiv:1207.7060
 Ting Y. S., Freeman K. C., Kobayashi C., De Silva G. M., Bland-Hawthorn J., 2012, MNRAS, 421, 1231
 Yanny B. et al., 2009, ApJ, 137, 4377